Impact of imperfect surface and imperfect groove pattern of compressor diffraction gratings on laser pulse focal intensity

Efim Khazanov

Gaponov-Grekhov Institute of Applied Physics of the Russian Academy of Sciences
Nizhny Novgorod, Russia

Abstract

An analytical expression for the focal intensity is derived for arbitrary surface profiles and arbitrary groove patterns of compressor gratings. The expression is valid for different compressor designs: plane and out-of-plane compressors, symmetric and asymmetric compressors (compressors composed by two not-identical pairs of grating), and a two-grating compressor. It is shown that the quality requirements for the optics used to write a grating are higher than for the grating. The focal intensity can be maximized by rotating each grating around its normal by 180 degrees. Moreover, it may be increased to maximum by interchanging any two gratings in the compressor, because imperfections of an individual grating do not additively affect the focal intensity. The intensity decrease is proportional to the squared pulse spectrum width and the squared total distortions of the second and third gratings of the four-grating compressor and the total distortions of two gratings of the two-grating compressor.

1. Introduction

The compressor in chirped pulse amplification lasers is one of the key elements of all high-power femtosecond lasers [1, 2]. Its main function is to compress the pulse to the Fourier limit, i.e. to obtain a pulse with a constant spectral phase at the output. In practice, an inevitable residual spectral phase is still crucial. To approach the Fourier limit, an acousto-optic programmable dispersive filter (AOPDF) [3] is used. The shortest pulse is a key goal, because it provides the highest pulse power for a given pulse energy. Nevertheless, the most important parameter is the focal intensity, which strongly depends on beam focusability. The highest focusability is provided by a diffraction limited beam, i.e. a beam with a plane wavefront (a flat spatial phase). To approach the diffraction limited beam, adaptive mirrors (AM) are widely employed [4]. AOPDF and AM efficiently correct temporal and spectral phase distortions separately, but they are not able to compensate for space-time coupling; therefore, the focal intensity is less than the diffraction limit. Besides the reduction of focal intensity (which is the subject of the present paper), the space-time coupling affects the pulse contrast ratio. The contrast degradation due to imperfect surface quality of stretcher and compressor optics was studied analytically [5-7], numerically [8-11] and experimentally [7, 10, 11].

Compressor diffraction gratings introduce two types of space-time coupling: amplitude and phase ones. The amplitude coupling is related to the spatial dependence of the reflection coefficient [12], as well as to the beam clipping on the gratings [12, 13], if any. In this paper, we will restrict our study to the phase space-time coupling caused by two reasons. The first one is an imperfectly flat grating surface. This effect was numerically studied in [12, 14-20], and an analytical expression for the focal intensity for arbitrary compressor grating surface profiles was obtained in [21].

10.1017/hpl.2025.10047

The second, much less studied reason for the phase space-time coupling is the groove pattern imperfection: non-equidistance and non-parallelism. In this case, the wavefront of the wave reflected from the grating is no longer flat, even for a perfectly flat surface, and the wavefront distortions are different for different frequencies, which results in space-time coupling. Methods for measuring groove imperfection of the grating were proposed in [22, 23]. For holographic gratings, groove imperfection is determined exclusively by the imperfect wavefronts of the waves used for writing the grating [24, 25]. The impact of groove imperfection on the compressor of femtosecond laser pulses was studied in [24], where only a particular case of period-chirped gratings was considered. The simplest case in which only the fourth grating of the classical Treacy compressor (TC) [26] is non-ideal was studied analytically in [23]. The TC consists of two identical pairs of diffraction gratings, where the gratings in each pair are parallel and the pairs are mirror images of each other, i.e. the TC is a plane symmetric compressor.

Recently, two routes of TC modification have been discussed in the literature. The first one – an asymmetric compressor – is based on abandoning symmetry, and the second – an out-of-plane compressor (OC) – is based on abandoning flat geometry. In the asymmetric compressor proposed in [27] two pairs of parallel diffraction gratings differ from each other by grating distance and/or incident angle. An important property of the asymmetric compressor is smoothing of fluence fluctuations, which allows a significant reduction of the probability of optical breakdown of the fourth grating. In [28], an analytical theory was constructed, which showed that no compressor asymmetry reduces focal intensity. This conclusion is also true for a compressor consisting of one pair of gratings, which is a special (maximum asymmetric) case [12, 29, 30]. In the OC [31-38], the angle of incidence in the plane normal to the diffraction plane is nonzero. In [39] it was shown that effective smoothing of the output beam is also possible in the OC, which was confirmed experimentally [40]. In [41] it was proposed to use the OC to increase the output power by reducing the angle of incidence.

In Section 2, the focal intensity will be found analytically for an arbitrary symmetric OC and a maximum asymmetric OC consisting of one pair of gratings. The influence of the grating surface profile imperfection will be compared with the impact of the groove pattern imperfection, and the symmetric compressor will be compared with the asymmetric one and the plane compressor with the OC in Section 3.

2. Dependence of focal intensity on out-of-plane compressor parameters

Let the compressor consist of gratings with groove density N and distance between the gratings along the normal L. We will consider the OC with the angle of incidence on the first grating α in the diffraction plane and γ in the non-diffraction plane. Most labs use a compressor consisting of two identical pairs of gratings: the parameters $a, \gamma, N,$ and L are the same for the two pairs. Such a compressor is referred to as a symmetric one (Fig. 1a). In an asymmetric compressor [27, 28, 39, 42] the grating pairs differ from each other; they have at least one of the parameters $a, \gamma, N,$ or L that differs from the others. The asymmetric compressor smooths small-scale fluence fluctuations and, hence, reduces the probability of laser induced damage. A special case of the asymmetric compressor is a compressor consisting of just one pair of gratings – a two-grating compressor (Fig. 1b) [13, 27, 30]. It has some additional advantages: smoothing of large-scale fluence fluctuations, simplicity, and lower cost. From the point of view of compressor (a)symmetry, we will restrict ourselves to two most interesting cases – a symmetric compressor and an asymmetric two-grating compressor (Fig. 1,a,b). They will be designated as 4OC (4-grating out-of-plane compressor) and 2OC (2-grating out-of-plane compressor). A plane Treacy compressor is a particular case of the OC at $\gamma = 0$, so it will be designated as 4TC and 2TC. Another interesting special case is the Littrow compressor, in which $\alpha = \alpha_L$, where α_L is the Littrow angle; the abbreviations 4LC and 2LC will be used for this compressor. The LC has a number of additional advantages [21, 33, 41]. We assume that the beam size and the size of gratings G2 and G3 are such that all frequencies fall

https://doi.org/10.1017/hpl.2025.10047 Published online by Cambridge University Press

into the aperture of G2 and G3, i.e. there are no beams that "miss" the grating. This is not the case for the so-called full-aperture compressor [13, 30, 43], which is not considered in this paper.

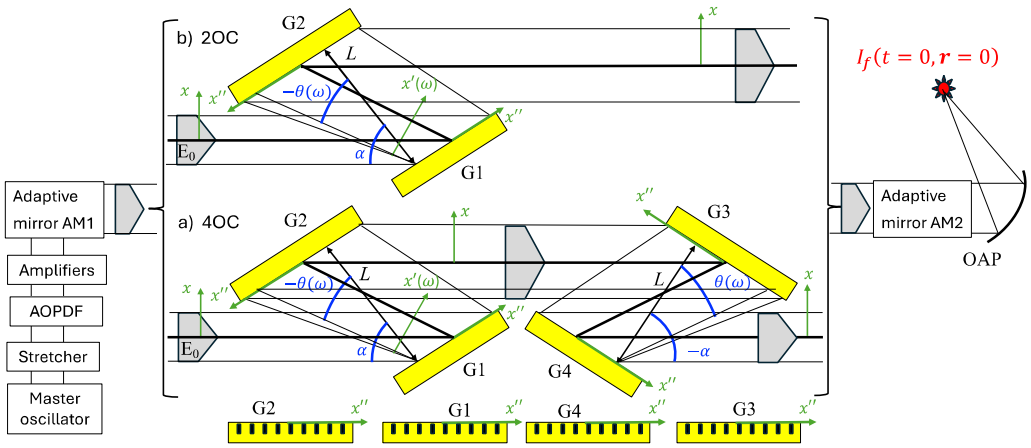

Fig. 1. 4OC (symmetric) (a) and 2OC (maximum asymmetric) (b). G1…G4 – gratings. OAP – off-axis parabola; $m = -1$; the angle of reflection from the first grating is negative. Angle γ is not shown as it is outside the plane of the figure, γ is the same for all gratings.

In the case of a perfect grating, the incident plane wave after reflection remains plane, i.e. its spatial phase $\Delta(x, y) = const$, and the angle of reflection $\theta(\omega)$ is determined by the expression for the grating

$$sin\theta(\omega) = m\frac{2\pi c}{\omega}\frac{N}{cos\gamma} + sin\alpha, \tag{1}$$

where m is the diffraction order. A perfect grating is understood as a grating with a perfectly flat substrate surface and perfectly parallel and equidistant grooves. As a result of an imperfect (out-of-plane) surface and imperfect (non-equidistant and non-parallel) grooves the wavefront of the reflected wave is no longer flat and $\Delta(x, y) \neq const$. Adaptive mirrors AM1,2 can compensate for distortions only at one (central) frequency ω_0. Since Δ depends on frequency ω (space-time coupling), this compensation cannot be complete, which leads to a decrease in the focal intensity. In [23], an expression was found for the spatial phase $\Delta(x', y', \omega)$ of a plane monochromatic wave after reflection from the grating:

$$\Delta(x', y', \omega) = -\frac{\omega}{c}\left(H_{gr}h_{gr}\left(\frac{x\prime}{cos\theta(\omega)}, \frac{y\prime}{cos\gamma}\right) + H_{wr}h_{wr}\left(\frac{x\prime cos}{cos\theta(\omega)}, \frac{y\prime}{cos\gamma}\right)\right), \tag{2}$$

where

$$H_{gr}(\omega) = cos\gamma\left(cos\alpha + cos\theta(\omega)\right), \qquad H_{wr}(\omega) = 2\frac{\omega_{wr}}{\omega}, \tag{3}$$

$h_{gr}(x'', y'')$ is the profile of the grating surface; $h_{wr}(x'', y'')$ characterizes groove pattern imperfection and has the sense of the difference of the total surface profiles of the optical elements on the path of two waves writing the holographic grating (Fig. 2); $\omega_{wr} = 2\pi c/\lambda_{wr}$ is the frequency of the writing waves; and Φ is the angle of incidence of the writing waves on the grating substrate $sin\Phi = N\lambda_{wr}/2$. Here, (x'', y'') are the coordinates of the grating surface and (x', y') are the coordinates in the plane normal to the wave vector of the beam between the first and second gratings shown in Fig.1. On reflection from the second grating, the beam changes its size, i.e. to pass to the laboratory reference frame, (x, y), x' in (2) must be replaced by $\frac{cos\theta(\omega)}{cos\alpha}x$. Thus, the phase introduced into the beam upon reflection from the first grating has a form:

https://doi.org/10.1017/hpl.2025.10047 Published online by Cambridge University Press

$$\Delta_1(x,y,\omega) = -\frac{\omega}{c}\left(H_{gr}h_{gr,1}\left(\frac{x}{cos\alpha},\frac{y}{cos\gamma}\right) + H_{wr}h_{wr,1}\left(\frac{xco}{cos\alpha},\frac{y}{cos\gamma}\right)\right) \quad (4)$$

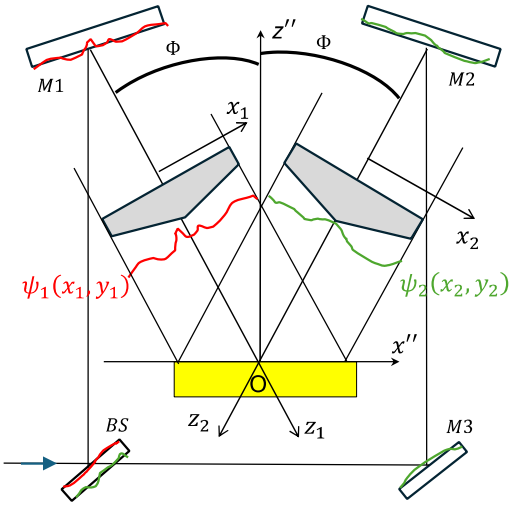

Fig. 2. Scheme of writing a holographic grating. BS – beamsplitter, M1…M3 – mirrors; $\psi_{1,2}$ – phase of the beams writing the grating; $\psi_1 - \psi_2 = 2k_{wr}h_{wr}$.

To find the phase for the remaining gratings, we fix the coordinate system (x'', y'') on each grating (Fig. 1) so that, in the case of identical gratings, the functions $h_{gr}(x'', y'')$ and $h_{wr}(x'', y'')$ should be identical for all gratings: $h_{gr} = h_{gr,n};\ h_{wr} = h_{wr,n}; n = 1,2,3,4$ is the grating number.

As can be seen from Fig. 1, for even gratings the angle between the x'' and x axes is obtuse; therefore, the sign of the first argument in h_{gr} and h_{wr} for them should be changed: $x \to -x$. Accordingly, for a grating with number n, the substitution $x \to (-1)^{n+1}x$ should be made in the right-hand side of (4). As shown in [23], the expression (2) is valid if the wave vector of the incident wave makes an acute angle with the x'' axis. If this angle is obtuse, then the plus sign in front of H_{wr} should be replaced with the minus sign. From Fig. 1 it is clear that G3 and G4 must have the minus sign. Therefore, in front of H_{wr} the factor $(-1)^{\left[\frac{n-1}{2}\right]}$ should be used, where […] denotes the integer part. In addition, for the second and fourth gratings in (2), obvious substitutions $\alpha \to -\theta(\omega)$ and $\theta(\omega) \to -\alpha$ should be made. Taking all this into account, the phase introduced by the reflection from the grating with number n takes on the form

$$\Delta_n(x,y,\omega) = -\frac{\omega}{c}\left(H_{gr}h_{gr,n}\left((-1)^{n+1}\frac{x}{cos\alpha},\frac{y}{cos\gamma}\right) + (-1)^{\left[\frac{n-1}{2}\right]}H_{wr}h_{wr,n}\left((-1)^{n+1}\frac{xcos\Phi}{cos\alpha},\frac{y}{cos\gamma}\right)\right) \quad (5)$$

Let the input field have the form

$$E_0(\omega,\boldsymbol{r}) = e^{i\varphi_{in}(\omega)+i\varphi_D(\omega)}e^{-\left(\frac{\omega-\omega_0}{\Delta\omega}\right)^{2\mu}}e^{iy\frac{\omega}{c}sin\gamma}|E_0(\boldsymbol{r})|\,, \quad (6)$$

where $\varphi_{in}(\omega)$ is the spectral phase without allowance for the phase introduced by the AOPDF $\varphi_D(\omega)$. Here we assume that the wavefront of $E_0(\boldsymbol{r})$ is plane, i.e. $E_0(\boldsymbol{r}) = |E_0(\boldsymbol{r})|$. If this is not the case, the first adaptive mirror AM1 can fix it. The Strehl ratio is defined by

$$St = \frac{I_f}{I_f(h_{gr}=h_{wr}=0)}, \quad (7)$$

where I_f is focal intensity. According to (7), the Strehl ratio shows the reduction of the focal intensity compared to the case of compressor gratings with perfectly plane surface and perfectly

https://doi.org/10.1017/hpl.2025.10047 Published online by Cambridge University Press

parallel and equidistant grooves. We assume that AM2 provides a plane wavefront at central frequency ω_0, and AOPDF ensures a constant spectral phase at zero spatial frequency $\kappa = 0$, as under these conditions I_f is maximal [21]. Following the procedure described in [21], in the $\left(\frac{\Delta\omega}{\omega_0}\right)^2 \overline{\Psi_{4,2}^2} \ll 2$ approximation for 4OC and 2OC we find St_2 and St_4:

$$St_{4,2} = 1 - M(\mu)\left(\frac{\Delta\omega}{\omega_0}\right)^2 \overline{\Psi_{4,2}^2(x,y)}\,, \tag{8}$$

where $M(\mu) = \Gamma\left(\frac{3}{2\mu}\right)/\Gamma\left(\frac{1}{2\mu}\right)$, Γ is the gamma function, $\overline{(\ldots)}$ denotes averaging over the grating surface with the weight of the laser field module:

$$\overline{(\ldots)} \equiv \frac{\int |E_0(x\cos\alpha, y\cos\ )|(\ldots)dxdy}{\int |E_0(x\cos\ , y\cos\ )|dxdy} \tag{9}$$

$$\Psi_4(x,y) = \frac{\omega_0}{c}\left(fg_4(x,y) + uw_4(x\cos\Phi, y) - \mathbf{FG}(x,y) - \mathbf{UW}(x\cos\Phi, y)\right) \tag{10}$$

$$\Psi_2(x,y) = \frac{\omega_0}{c}\left(fg(x,y) + uw(x\cos\Phi, y)\right) \tag{11}$$

$$g_4(x,y) = \sum_{n=1}^{4} h_{gr,n}\left((-1)^{n+1}x, y\right) \qquad w_4(x,y) = \sum_{n=1}^{4}(-1)^{\left[\frac{n-1}{2}\right]} h_{wr,n}\left((-1)^{n+1}x, y\right) \tag{12}$$

$$g(x,y) = h_{gr,1}(x,y) + h_{gr,2}(-x,y) \qquad w(x,y) = h_{wr,1}(x,y) + h_{wr,2}(-x,y) \tag{13}$$

$$\mathbf{G}(x,y) = \boldsymbol{\nabla} h_{gr,2}(-x,y) + \boldsymbol{\nabla} h_{gr,3}(x,y) \qquad \mathbf{W}(x,y) = -\boldsymbol{\nabla} h_{wr,2}(-x,y) - \boldsymbol{\nabla} h_{wr,3}(x,y) \tag{14}$$

$$f = 2\pi N tg\beta \qquad u = \frac{4\pi}{\lambda_{wr}} \qquad \mathbf{F} = 2\pi NL\frac{\cos\alpha + \cos\beta}{\cos\gamma\cos^3\beta}\begin{pmatrix}\cos\alpha\cos\gamma \\ \lambda_0 N tg\gamma\end{pmatrix} \qquad \mathbf{U} = 2\frac{tg\left(\frac{\alpha-\beta}{2}\right)}{N\lambda_{wr}}\mathbf{F} \tag{15}$$

$$\boldsymbol{\nabla} h(-x,y) \triangleq \boldsymbol{\nabla} h(x,y)|_{x=-x}\ , \tag{16}$$

$\beta = \theta(\omega_0)$. Hereafter, the sub-indices "2" and "4" correspond to the two-grating (Fig. 1b) and the four-grating (Fig. 1a) compressors. The sub-index "4,2" denotes either the four-grating or the two-grating compressor. Without loss of generality, hereinafter we assume that $\bar{g} = \overline{w} = \overline{g_4} = \overline{w_4} = \overline{\boldsymbol{G}} = \overline{\mathbf{W}} = 0$. In addition, the functions $h_{gr,n}$ and $h_{wr,n}$ do not contain components linear with respect to x and y (wedges) that are equivalent to the rotation of the grating as a whole for $h_{gr,n}$ and to the changes in the groove density N uniformly over the entire grating surface for $h_{wr,n}$. As shown in [21], all the components in $\boldsymbol{\nabla} h_{gr,n}(x,y)$ linear with respect to x and y can be effectively compensated for by rotating one grating, for example, G4. The same is true for $\boldsymbol{\nabla} h_{wr,n}(x,y)$. If this is done, then the terms linear with respect to x and y should be subtracted from $\boldsymbol{\nabla} h_{gr,n}(x,y)$ and $\boldsymbol{\nabla} h_{wr,n}(x,y)$ in (14). These terms correspond to the aberrations of $h_{gr,n}(x,y)$ and $h_{wr,n}(x,y)$ quadratic with respect to x and y, i.e. to defocus, vertical astigmatism, and oblique astigmatism.

Taking into account that $|\boldsymbol{\nabla} h_n(x,y)| \approx \frac{h_n(x,y)}{d}$, where $d < \frac{L_g}{2}$ is a typical transverse scale of $h_i(x,y)$ variation, and that $L_g < L$, we obtain

$$\frac{fg_4(x,y)}{\mathbf{FG}(x,y)} \leqslant \frac{\sin\beta\cos^2\beta}{2(\cos\alpha+\cos\beta)\cos\alpha}\frac{L_g}{L} \ll 1 \qquad \frac{uw_4}{\mathbf{UW}} \leqslant \frac{ctg\left(\frac{\alpha-\beta}{2}\right)\cos^3\beta}{2(\cos\alpha+\cos\beta)\cos\alpha}\frac{L_g}{L} \ll 1 \tag{17}$$

and the expression (10) reduces to

$$\Psi_4(x,y) = -\frac{\omega_0}{c}\left(\mathbf{FG}(x,y) + \mathbf{UW}(x\cos\Phi, y)\right) \tag{18}$$

Let us now consider this case and use (18) for 4OC. It should be noted, however, that the above approximation is violated if the quadratic components in $h_{gr,n}(x,y)$ and $h_{wr,n}(x,y)$ are significantly larger than all the others taken together. Then, if the quadratic distortions are

https://doi.org/10.1017/hpl.2025.10047 Published online by Cambridge University Press

compensated for by rotating the fourth grating [21], the approximation $|\boldsymbol{\nabla} h_n(x,y)| \approx \frac{h_n(x,y)}{d}$ is invalid and (10) must be used instead of (18).

As seen from (18), the focal intensity for 4OC is determined by the total value of the h_{gr} and h_{wr} gradients (functions $\mathbf{G}(x,y)$ and $\mathbf{W}(x,y)$), where only gratings G2 and G3 are significant, whereas the contribution of G1 and G4 is negligible. Contrariwise, for 2OC, according to (11), the gradients are of no importance, and the focal intensity is determined only by the total value of h_{gr} and h_{wr} (functions $g(x,y)$ and $w(x,y)$).

Analogously to (17), we obtain $fg(x,y) \ll \mathbf{FG}(x,y)$ and $uw(x,y) \ll \mathbf{UW}(x,y)$. With allowance for (11) and (18), from this follows that a decrease in the Strehl ratio in 2OC is much smaller than in 4OC: $(1-St_2) \ll (1-St_2)$, which is a significant advantage of the two-grating compressor along with its other merits [21, 33, 41].

3. Discussion of results

As can be seen from (8), one function $\Psi_{4,2}(x,y)$ is responsible for all distortions of all compressor gratings. It has the meaning of the effective phase (effective wavefront), which characterizes all imperfections of all compressor gratings. The decrease in the Strehl ratio $\left(1-St_{4,2}\right)$ is proportional to the squared rms of this phase and to the squared $\Delta\omega$. Therefore, a decrease/increase in $\Delta\omega$ proportionally reduces/increases the requirements for the rms of both, the surface of the gratings and the surfaces of the optics used for their writing. To determine the Strehl ratio it is sufficient to know only $\overline{\Psi_{4,2}^2(x,y)}$, i.e. the dispersion (rms squared) of the function $\Psi_{4,2}(x,y)$, with averaging being performed according to (9). The laser beam profile $E_0(x,y)$ affects $St_{4,2}$ only through this averaging. It is obvious that the flat-top profile is better than the Gaussian one, especially in the presence in $\Psi_{4,2}(x,y)$ of Zernike polynomials with large radial indices. The pulse spectrum profile has a similar effect: for a Gaussian spectrum $M(\mu=1)=0.5$ and for $\mu \geq 6$, $M \approx 0.32$, i.e. for a super-Gaussian spectrum $St_{4,2}$ is larger than for a Gaussian one.

The function $\Psi_{4,2}(x,y)$ is determined by the total distortions of gratings G2 and G3 for 4OC (14) and G1 and G2 for 2OC (13). The rotation of one grating by 180 degrees around its normal changes the sign of the arguments of the functions $h_{gr}(x,y)$ and $h_{wr}(x,y)$. In addition, with such a rotation, the angle between the wave vector of the incident wave and the x'' axis changes from the acute to the obtuse one or vice versa, i.e. $h_{wr,n}(x,y)$ changes its sign [23]. Thus, the rotation corresponds to the replacements

$$h_{gr,n}(x,y) \to h_{gr,n}(-x,-y) \quad \text{and} \quad h_{wr,n}(x,y) \to -h_{wr,n}(-x,-y) \tag{19}$$

In 2OC the gratings may be arranged in four non-equivalent ways: each grating may be placed in two ways. There are significantly more options in 4OC. The values of $\overline{\Psi_{4,2}^2(x,y)}$ and, hence, of $St_{4,2}$ will be different for different variants. Knowing $h_{gr,n}(x,y)$ and $h_{wr,n}(x,y)$ for each grating, for any compressor it is easy to choose the best option – the one that gives the smallest value of $\overline{\Psi_{4,2}^2(x,y)}$.

The grating surface profiles $h_{gr,n}(x,y)$ are, as a rule, independent for different gratings. On the contrary, it is reasonable to conjecture that $h_{wr,n}(x,y) = h_{wr}(x,y)$, if the gratings are written by the same optics (see Fig. 2). Then, from (13, 14) we obtain

$$w(x,y) = h_{wr}(x,y) + h_{wr}(-x,y), \qquad \mathbf{W}(x,y) = -\boldsymbol{\nabla} h_{wr}(-x,y) - \boldsymbol{\nabla} h_{wr}(x,y), \tag{20}$$

https://doi.org/10.1017/hpl.2025.10047 Published online by Cambridge University Press

i.e. the Zernike polynomials that are odd in x will make a zero contribution to $w(x,y)$, and even ones a zero contribution to $\mathbf{W}(x,y)$ (see (16)). If the second grating is rotated by 180 degrees around its normal, then

$$w(x,y) = h_{wr}(x,y) - h_{wr}(x,-y), \qquad \mathbf{W}(x,y) = -\boldsymbol{\nabla} h_{wr}(-x,y) + \boldsymbol{\nabla} h_{wr}(-x,-y) \quad (21)$$

and the Zernike polynomials that are even in y will make a zero contribution to $w(x,y)$, and the odd ones to $\mathbf{W}(x,y)$. From this it is clear that identical gratings do not allow compensating for the imperfection of the grooves of each other, since in any case $w(x,y) \neq 0$ and $\mathbf{W}(x,y) \neq 0$. However, $w(x,y) = 0$ if any of the conditions

$$h_{wr,2}(x,y) = -h_{wr,1}(-x,y) \quad \text{or} \quad h_{wr,2}(x,y) = h_{wr,1}(x,-y) \quad (22)$$

is met, and $\mathbf{W}(x,y) = 0$ if any of the conditions

$$\boldsymbol{\nabla} h_{wr,2}(x,y) = -\boldsymbol{\nabla} h_{wr,1}(-x,y) \quad \text{or} \quad \boldsymbol{\nabla} h_{wr,2}(-x,-y) = \boldsymbol{\nabla} h_{wr,1}(-x,y) \quad (23)$$

is fulfilled. Thus, to completely nullify the influence of an imperfect groove pattern for 2OC or 4OC, a pair of grooves satisfying (22) or (23), respectively, should be written. By interchanging BS and M3, as well as M1 and M2 (Fig. 2), it is possible to change the sign of h_{wr}, but this is insufficient to fulfill (22, 23).

The Strehl ratio St depends on *i)* the total grating profile described by the functions $\mathbf{G}(x,y)$ and $g(x,y)$, and *ii)* the total groove imperfection which, in its turn, is determined by the total profile of the optics used for writing the grooves that is described by the functions $\mathbf{W}(x,y)$ and $w(x,y)$. Compare the influence of these two reasons assuming that the profiles are uncorrelated, i.e. $\overline{\boldsymbol{GW}} = \overline{gw} = 0$. Then from (8, 11, 18) we find that the Strehl ratio St is a product of the Strehl ratio caused by the grating surface imperfection St_{gr} and the Strehl ratio caused by the groove pattern imperfection St_{wr}:

$$St_4 = St_{4,gr} St_{4,wr} \qquad St_2 = St_{2,gr} St_{2,wr} \quad (24)$$

$$St_{4,gr} = 1 - \mathrm{M}\left(\frac{\Delta\omega}{\omega_0}\right)^2 \left(F_x^2 \overline{G_x^2} + F_y^2 \overline{G_y^2}\right) \qquad St_{4,wr} = 1 - \mathrm{M}\left(\frac{\Delta\omega}{\omega_0}\right)^2 \left(U_x^2 \overline{W_x^2} + U_y^2 \overline{W_y^2}\right) \quad (25)$$

$$St_{2,gr} = 1 - \mathrm{M}\left(\frac{\Delta\omega}{\omega_0}\right)^2 f^2 \overline{g^2} \qquad St_{2,wr} = 1 - \mathrm{M}\left(\frac{\Delta\omega}{\omega_0}\right)^2 u^2 \overline{w^2} \quad (26)$$

Note that for the St close to unity, the contribution of these two factors to the reduction of the Strehl ratio is additive: $1 - St \approx 1 - St_{gr} - St_{wr}$. Supposing that the quality of grating substrate polishing is the same as the quality of polishing the optics used for writing the grating, we have $\overline{g^2} = \overline{w^2} = \sigma^2$ and $\overline{G_x^2} = \overline{W_x^2} = \overline{G_y^2} = \overline{W_y^2} = \Sigma^2$. We also assume that x and y are equivalent. Then it is readily found that

$$\frac{1-St_{2,gr}}{1-St_{2,wr}} = \frac{1}{2} tg\beta N\lambda_{wr} \qquad \frac{1-St_{4,gr}}{1-St_{4,wr}} = \frac{1}{2} ctg\left(\frac{\alpha-\beta}{2}\right) N\lambda_{wr}$$

For typical compressor parameters, both ratios are << 1, i.e. the imperfection of the optics used to write the grating exerts a greater influence. For example, for the 4TC and 4LC parameters proposed in [41] for the XCELS and SEL-100PW projects (Table 1), $St_{4,gr}(\Sigma)$ and $St_{4,wr}(\Sigma)$ are plotted in Fig. 3, from which it is clear that $St_{4,gr}(\Sigma) \approx St_{4,wr}\big((2.5 \ldots 3)\Sigma\big)$, i.e. the requirements for the optics used to write the grating are approximately 2.5…3 times higher. The curves are plotted for $\lambda_{wr} = 413$ nm; for $\lambda_{wr} = 266$ nm this coefficient will be even 1.55 times larger.

Table 1. Compressor parameters

	XCELS	SEL-100PW
	910±75nm	925±100nm

https://doi.org/10.1017/hpl.2025.10047 Published online by Cambridge University Press

	4TC	4LC	4TC	4LC
N, mm^{-1}	950	1000	1000	1100
α, degree	36	27.4	38.5	31.3
γ, degree	0	11.2	0	14.8
L, cm	333	231	272	155

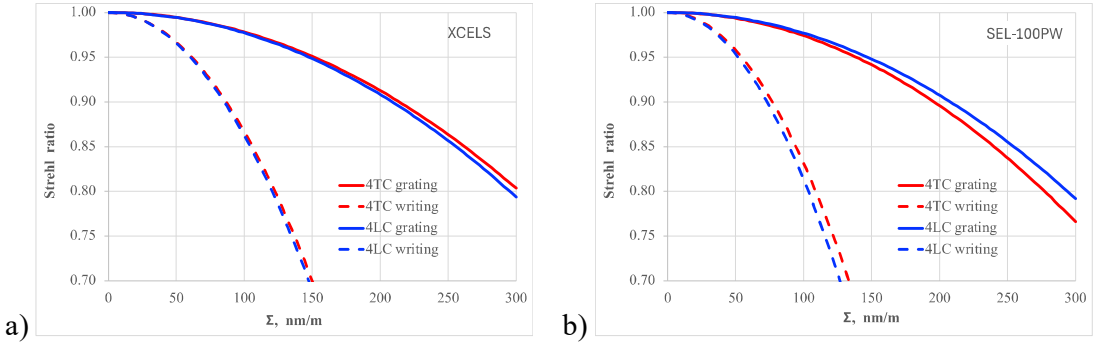

Fig. 3. $St_{4,gr}(\Sigma)$ (solid curves) and $St_{4,wr}(\Sigma)$ (dashed curves) plotted by (25) for 4TC (red) and 4LC (blue) for compressor parameters (see Table 1) proposed for XCELS (a) and SEL-100PW (b).

From (15) it is clear that u does not depend on N and the dependence of $\mathbf{U}$ on N is very weak. Consequently, $St_{wr,4}$ weakly depends on N, and $St_{wr,2}$ does not depend on it at all. Contrariwise, f and $\mathbf{F}$ and, hence, St_{gr} depend on N. In Fig. 4, $St_{gr}(N)$ and $St_{wr}(N)$ are plotted for four compressor configurations: 4TC, 4LC, 2TC and 2LC. For the TC, $\gamma = 0$ and the value of $|\alpha - \alpha_L|$ for each N was chosen to be minimal, ensuring decoupling (grating G2 does not overlap the beam incident on grating G1). Analogously, for LC the angle γ was chosen to be minimal and $\alpha = \alpha_L$. For all points in Fig.4 the distance between the gratings L corresponds to the group velocity dispersion of 4.4ps^2. For identical Σ and σ, the values of $St_{gr}(N)$ differ little from unity. Therefore, for clarity, the curves for $St_{gr}(N)$ are plotted a factor of 10 larger for Σ (Fig. 4a) and a factor of 5 larger for σ (Fig. 4b) than for $St_{wr}(N)$. This once again emphasizes that the contribution of h_{wr} is much larger than that of h_{gr}. As expected, St_{wr} (green symbols) is virtually independent of N, except for a small drop at large N in Fig. 4a. For the same quality of the optics, $St_{gr}(N) \approx 1$ and $St(N) \approx St_{wr}(N)$. However, if (22) is met or quadratic components (defocus, vertical astigmatism, and oblique astigmatism) dominate in h_{wr}, then $St_{wr}(N) \approx 1$ and $St(N) \approx St_{gr}(N)$. In this case, as can be seen from Fig. 4, for 4TC and 4LC it is more advantageous to have large N, and for 2TC and 2LC small N. The comparison of TC and LC (triangles vs squares) shows that St is larger for TC, but the difference is insignificant, and for the two-grating compressor St_{wr} is the same for 2TC and 2LC (circles in Fig.4b).

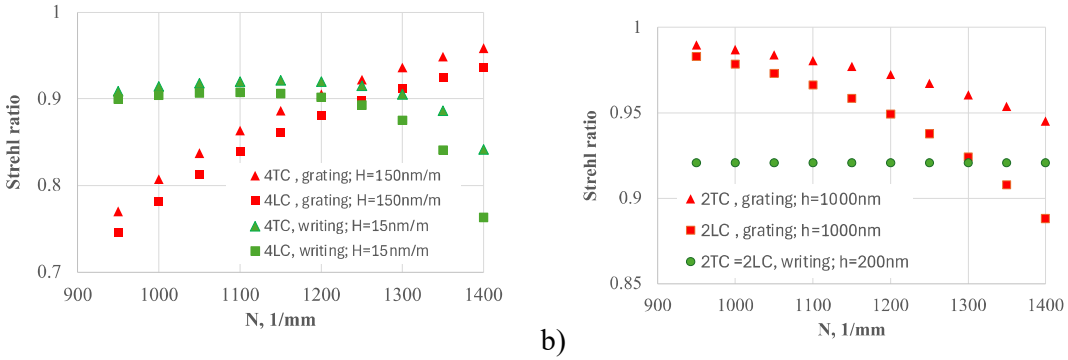

https://doi.org/10.1017/hpl.2025.10047 Published online by Cambridge University Press

Fig. 4. $St_{gr}(N)$ (red) and $St_{wr}(N)$ (green) for 4TC and 4LC plotted by (25) (a) and for 4TC , 2TC plotted by (25) and 2LC plotted by (26) (b). The incidence angles α and γ as well as the distance between the gratings L are described in the text. For clarity, the curves for $St_{gr}(N)$ are plotted for larger values of distortion than for $St_{wr}(N)$: a factor of 10 for (a) and a factor of 5 for (b).

4. Conclusion

The focal intensity (Strehl ratio St) depends on the grating surface profile $h_{gr}(x, y)$ and on the groove pattern imperfection $h_{wr}(x, y)$ – the function which, in turn, is determined by the total surface profile of the optics used for writing the holographic gratings. In the majority of cases, the influence of $h_{wr}(x, y)$ is much more significant, i.e. the requirements for the quality of the surface of the optics used for inscribing the gratings are several times higher than for the quality of the grating surface.

When the grating is rotated by 180 degrees around its normal, $h_{wr}(x, y)$ (unlike $h_{gr}(x, y)$) changes its sign. By rotating the gratings and interchanging them it is possible to find an optimal variant for maximizing St.

The influence of all imperfections of all compressor gratings on St is described by one function $\Psi(x, y)$ that has the sense of the effective wavefront. The decrease in St is proportional to the squared rms of this function. The $\Psi(x, y)$ function is determined by the total distortions of gratings G2 and G3 for the four-grating compressor (14) and of G1 and G2 for the two-grating compressor (13), with the St decrease in the latter being much smaller, which is its undoubted advantage.

The number of grooves N almost does not affect the decrease in St due to groove pattern imperfection, but it influences the St decrease due to the imperfection of the grating surface. In four-grating compressors, St increases with increasing N, while in two-grating compressors it decreases. The comparison of the Treacy and Littrow compressors demonstrated that St is higher for the Treacy compressor but the difference is insignificant.

In all cases the reduction of the pulse spectrum width $\Delta\omega$ proportionally reduces the requirements for the rms of both, the surface of the gratings and the surface of the optics used for their writing.

https://doi.org/10.1017/hpl.2025.10047 Published online by Cambridge University Press

References

1. C. Danson, J. Bromage, T. Butcher, J.-C. Chanteloup, E. Chowdhury, A. Galvanauskas, L. Gizzi, C. Haefner, J. Hein, D. Hillier, N. Hopps, Y. Kato, E. Khazanov, R. Kodama, G. Korn, R. Li, Y. Li, J. Limpert, J. Ma, C. H. Nam, D. Neely, D. Papadopoulos, R. Penman, L. Qian, J. Rocca, A. Shaykin, C. Siders, C. Spindloe, S. Szatmári, R. Trines, J. Zhu, P. Zhu, and J. Zuegel, "Petawatt and exawatt class lasers worldwide", High Power Laser Science and Engineering **7**, e54 (2019) https://doi.org/10.1017/hpl.2019.36Published
2. Z. Li, Y. Leng, and R. Li, "Further development of the short-pulse Petawatt laser: trends, technologies, and bottlenecks", Laser & Photonics Review **7**, 2100705 (2022) 10.1002/lpor.202100705.
3. P. Tournois, "Acousto-optic programmable dispersive filter for adaptive compensation of group delay time dispersion in laser systems", Optics Communications **140**, 245-249 (1997) https://doi.org/10.1016/S0030-4018(97)00153-3.
4. V. Samarkin, A. Alexandrov, G. Borsoni, T. Jitsuno, P. Romanov, A. Rukosuev, and A. Kudryashov, "Wide aperture piezoceramic deformable mirrors for aberration correction in high-power lasers", High Power Laser Science and Engineering **4**, e4 (2016) https://doi.org/10.1017/hpl.2016.3.
5. C. Dorrer and J. Bromage, "Impact of high-frequency spectral phase modulation on the temporal profile of short optical pulses", Optics Express **16**, 3058-3068 (2008)
6. J. Bromage, C. Dorrer, and R. K. Jungquist, "Temporal contrast degradation at the focus of ultrafast pulses from high-frequency spectral phase modulation", JOSA B **29**, 1125-1135 (2012) •https://doi.org/10.1364/JOSAB.29.001125.
7. S. Roeder, Y. Zobus, C. Brabetz, and V. Bagnoud, "How the laser beam size conditions the temporal contrast in pulse stretchers of chirped-pulse amplification lasers", High Power Laser Science and Engineering **10**, e34 (2022) doi:10.1017/hpl.2022.18.
8. V. Bagnoud and F. Salin, "Influence of optical quality on chirped-pulse amplification: characterization of a 150-nm-bandwidth stretcher", J. Opt. Soc. Am. B **16**, 188-193 (1999) •https://doi.org/10.1364/JOSAB.16.000188.
9. B. Webb, C. Feng, C. Dorrer, C. Jeon, R. G. Roides, S. Bucht, and J. Bromage, "Degradation of temporal contrast from post-pedestal interference with a chirped pulse in an optical parametric amplifier", Optics Express **32**, 12276-12290 (2024) •https://doi.org/10.1364/OE.518096.
10. B. Webb, C. Dorrer, S.-W. Bahk, C. Jeon, R. G. Roides, and J. Bromage, "Temporal contrast degradation from mid-spatial-frequency surface error on stretcher mirrors", Applied Optics **63**, 4615-4621 (2024) https://doi.org/10.1364/AO.522892.
11. Z. Li, S. Tokita, S. Matsuo, K. Sueda, T. Kurita, T. Kawasima, and N. Miyanaga, "Scattering pulse-induced temporal contrast degradation in chirped-pulse amplification lasers", Optics Express **25**, 21201-21215 (2017) •https://doi.org/10.1364/OE.25.021201.
12. Z. Li, J. Liu, Y. Xu, Y. Leng, and R. Li, "Simulating spatiotemporal dynamics of ultra-intense ultrashort lasers through imperfect grating compressors", Optics Express **30**, 41296-41312 (2022) https://doi.org/10.1364/OE.473439.
13. A. Vyatkin and E. Khazanov, "Grating compressor optimization aiming at maximum focal intensity of femtosecond laser pulses", Optics Express **32**, 39394-39407 (2024) •https://doi.org/10.1364/OE.535150.
14. Z. Li and J. Kawanaka, "Complex spatiotemporal coupling distortion pre-compensation with double-compressors for an ultra-intense femtosecond laser", Opt. Express **27**, 25172-25186 (2019) doi.org/10.1364/OE.27.025172.
15. Z. Li and N. Miyanaga, "Simulating ultra-intense femtosecond lasers in the 3-dimensional space-time domain", Optics Express **26**, 8453-8469 (2018) 10.1364/OE.26.008453.
16. V. Leroux, T. Eichner, and A. R. Maier, "Description of spatio-temporal couplings from heat-induced compressor grating deformation", Opt Express **28**, 8257-8265 (2020) 10.1364/OE.386112.

https://doi.org/10.1017/hpl.2025.10047 Published online by Cambridge University Press

17. J. Qiao, J. Papa, and X. Liu, "Spatio-temporal modeling and optimization of a deformable-grating compressor for short high- energy laser pulses", Opt. Express **23**, 25923-25934 (2015) 10.1364/OE.23.025923.
18. Z. Li, K. Tsubakimoto, H. Yoshida, Y. Nakata, and N. Miyanaga, "Degradation of femtosecond petawatt laser beams: Spatio-temporal/spectral coupling induced by wavefront errors of compression gratings", Applied Physics Express **10**, 102702 (2017) https://doi.org/10.7567/APEX.10.102702.
19. J. Liu, X. Shen, Z. Si, C. Wang, C. Zhao, X. Liang, Y. Leng, and R. Li, "In-house beam-splitting pulse compressor for high-energy petawatt lasers", Optics Express **28**, 22978-22991 (2020) https://doi.org/10.1364/OE.398668.
20. J. Liu, X. Shen, S. Du, and R. Li, "A multistep pulse compressor for 10s to 100s PW lasers", Optics Express **29**, 17140-17158 (2021) 10.1364/OE.424356.
21. E. Khazanov, "Dependence of the focal intensity of a femtosecond laser pulse on the non-flatness of compressor diffraction gratings", High Power Laser Science and Engineering **12**, e85 (2024) doi:10.1017/hpl.2024.58.
22. F. Bienert, C. Röcker, T. Graf, and M. A. Ahmed, "Simple spatially resolved period measurement of chirped pulse compression gratings", Optics Express **31**, 19392-19403 (2023) •https://doi.org/10.1364/OE.489238.
23. E. Khazanov, "Wavefront distortions of a laser beam reflected from a diffraction grating with imperfect surface and groove pattern ", Optics Express **32**, 46310 (2024) https://doi.org/10.1364/OE.542565.
24. F. Bienert, C. Röcker, T. Dietrich, T. Graf, and M. A. Ahmed, "Detrimental effects of period-chirped gratings in pulse compressors", Optics Express **31**, 40687-40704 (2023) https://doi.org/10.1364/OE.505875.
25. N. Bonod and J. Neauport, "Diffraction gratings: from principles to applications in high-intensity lasers", Advances in Optics and Photonics **8**, 156-199 (2016) •https://doi.org/10.1364/AOP.8.000156.
26. E. B. Treacy, "Optical pulse compression with diffraction gratings", IEEE Journal of Quantum Electronics **QE-5**, 454-458 (1969)
27. X. Shen, S. Du, W. Liang, P. Wang, J. Liu, and R. Li, "Two-step pulse compressor based on asymmetric four-grating compressor for femtosecond petawatt lasers", Applied Physics B **128**, 159 (2022) https://doi.org/10.1007/s00340-022-07878-9.
28. E. Khazanov, "Reducing laser beam fluence and intensity fluctuations in symmetric and asymmetric compressors", High Power Laser Science and Engineering **11**, e93 (2023) doi:10.1017/hpl.2023.83.
29. S. Du, X. Shen, W. Liang, P. Wang, J. Liu, and R. Li, "A 100-PW compressor based on single-pass single-grating pair", High Power Laser Science and Engineering **11**, e4 (2023) 10.1017/hpl.2023.5.
30. M. Trentelman, I. N. Ross, and C. N. Danson, "Finite size compression gratings in a large aperture chirped pulse amplification laser system", Applied Optics **36**, 8567-8573 (1997) 10.1364/ao.36.008567.
31. K. Osvay and I. N. Ross, "On a pulse compressor with gratings having arbitrary orientation", Optics Communications **105**, 271-278 (1994)
32. G. Kalinchenko, S. Vyhlidka, D. Kramer, A. Lererc, and B. Rus, "Positioning of Littrow mounted gratings in pulse compressors," in Optical Systems Design 2015,(Jena, Germany) Proc. SPIE v. 9626 96261R-96261, (2015) 10.1117/12.2191304.
33. D. L. Smith, S. L. Erdogan, and T. Erdogan, "Advantages of out-of-plane pulse compression gratings", Applied Optics **62**, 3357-3369 (2023) https://doi.org/10.1364/AO.485637.
34. Y. Han, H. Cao, F. Kong, Y. Jin, and J. Shao, "All- and mixed-dielectric grating for Nd:glass-based high-energy pulse compression", High Power Laser Science and Engineering **11**, e60 (2023) 10.1017/hpl.2023.39.
35. L. Li, "Propagating-order scattering matrix of conically mounted and crossed gratings", Journal of the Optical Society of America A **38**, 426-436 (2021) https://doi.org/10.1364/JOSAA.417769.

36. K. Wei and L. Li, "Spectral beam combining gratings: high diffraction efficiency at a large deviation angle achieved around conical Littrow mounting", Optics Letters **46**, 4626-4629 (2021) https://doi.org/10.1364/OL.440150.
37. Š. Vyhlídka, P. Trojek, D. Kramer, D. Peceli, F. Batysta, J. Bartoníček, J. Hubáček, T. Borger, R. Antipenkov, E. Gaul, T. Ditmire, and B. Rus, "Temporal diagnostics for kJ class laser using object-image-grating self-tiling compressor," in Short-pulse High-energy Lasers and Ultrafast Optical Technologies,(Prague, Czech Republic) Proc. SPIE v.11034, 1103409, (2019) 10.1117/12.2524484.
38. C. M. Werle, C. Braun, T. Eichner, T. Hulsenbusch, G. Palmer, and A. R. Maier, "Out-of-plane multilayer-dielectric-grating compressor for ultrafast Ti:sapphire pulses", Optics Express **31**, 37437-37451 (2023)
39. E. Khazanov, "2D-smoothing of laser beam fluctuations in optical compressor", Laser Phys. Lett. **20**, 125001 (2023) https://doi.org/10.1088/1612-202X/ad00ab.
40. D. E. Kiselev, A. A. Kochetkov, I. V. Yakovlev, and E. A. Khazanov, "Experimental study of laser beam fluence fluctuation smoothing in asymmetric compressors", Applied Optics **63**, 9146-9151 (2024) https://doi.org/10.1364/AO.542361.
41. E. Khazanov, "New grating compressor designs for XCELS and SEL-100 PW projects", High Power Laser Science and Engineering **12**, e36 (2024) 10.1017/hpl.2024.18.
42. H. Huang and T. Kessler, "Tiled-grating compressor with uncompensated dispersion for near-field-intensity smoothing", Optics Letters **32**, 1854-1856 (2007) •https://doi.org/10.1364/OL.32.001854.
43. C. Wang, D. Wang, Y. Xu, and Y. Leng, "Full-aperture chirped-pulse grating compression with a non-uniform beam", Optics Communications **507**, 127613 (2022) https://doi.org/10.1016/j.optcom.2021.127613.

https://doi.org/10.1017/hpl.2025.10047 Published online by Cambridge University Press